

See discussions, stats, and author profiles for this publication at: <https://www.researchgate.net/publication/262143206>

Atomic Layer Deposition Preparation of Pd Nanoparticles on a Porous Carbon Support for Alcohol Oxidation

ARTICLE in THE JOURNAL OF PHYSICAL CHEMISTRY C · OCTOBER 2011

Impact Factor: 4.77 · DOI: 10.1021/jp2083659

CITATIONS

32

READS

34

9 AUTHORS, INCLUDING:



Maryam Borghei

Aalto University

23 PUBLICATIONS 302 CITATIONS

[SEE PROFILE](#)



Ville Viitanen

6 PUBLICATIONS 59 CITATIONS

[SEE PROFILE](#)



Jani Sainio

Aalto University

47 PUBLICATIONS 793 CITATIONS

[SEE PROFILE](#)



Tanja Kallio

Aalto University

87 PUBLICATIONS 947 CITATIONS

[SEE PROFILE](#)

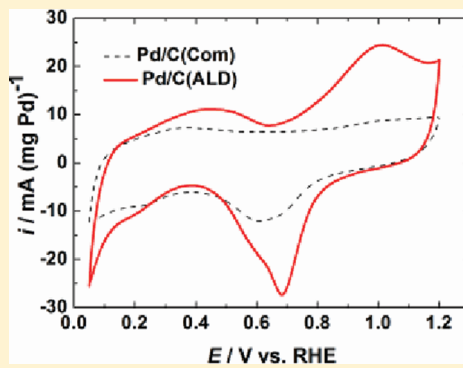
Atomic Layer Deposition Preparation of Pd Nanoparticles on a Porous Carbon Support for Alcohol Oxidation

Emma Rikkinen,^{*,†} Annukka Santasalo-Aarnio,[‡] Sanna Airaksinen,[†] Maryam Borghei,[§] Ville Viitanen,^{||} Jani Sainio,^{||} Esko I. Kauppinen,[†] Tanja Kallio,[‡] and A. Outi I. Krause[†]

[†]Industrial Chemistry Research Group and [‡]Fuel Cell Research Group, School of Chemical Technology, and [§]NanoMaterials Group and ^{||}Department of Applied Physics, School of Science, Aalto University, FI-00076 AALTO, Finland

 Supporting Information

ABSTRACT: To reduce the loading of noble metals on fuel cell catalysts a synthesis method providing evenly distributed nanoparticles on the support surface is needed. Narrow size distribution palladium nanoparticles were prepared on a porous carbon support by atomic layer deposition (ALD), and their activity for ethanol and isopropanol oxidation was studied electrochemically in alkaline media. Palladium particles had smaller average particle sizes on the support material resulting in ~ 50 mV lower onset potential and 2.5 times higher mass activity for alcohol oxidation compared with a commercial catalyst. The results indicate that the use of ALD allows the preparation of a noble metal nanoparticle catalyst, and this catalyst can provide similar mass activity with lower catalyst loading than current commercial fuel cell catalysts. This would significantly reduce the cost of the cell and provide a competitive advantage compared with other power sources.



INTRODUCTION

Direct alcohol fuel cells (DAFCs) are promising energy sources for low-power demand devices such as laptops and mobile phones. However, the reaction rate of sluggish alcohol oxidation at the anode is still one of the key factors preventing their commercialization.¹ The reaction rate can be enhanced in alkaline media,^{2–5} and the interest in alkaline DAFCs has recently increased because of the development of anion exchange membranes.^{6–9} For further enhancement, alcohol oxidation noble metals can be used as catalysts. In acidic media, platinum is most commonly applied as an electrocatalyst by itself or as an alloy; however, in alkaline media palladium has also shown high activity, especially for ethanol and isopropanol oxidation.^{10,11} These alcohols are interesting alternatives to the widely used methanol because of their lower crossover rate,^{12,13} higher boiling points, lower toxicity, and high performance in preliminary fuel cell tests.^{5,12,14} Currently, most noble metal catalysts used in fuel cell applications are produced using a liquid–solid nanoparticle synthesis that results in inhomogeneous catalyst materials that affect dramatically the particle size distribution and electrochemically active surface area (EASA) of the catalyst. Because of the high cost and low availability of noble metals the loading on the catalyst must be decreased if DAFCs are to compete with other power sources in commercial applications.

Atomic layer deposition (ALD) is a method for preparing thin films on planar substrates and on porous materials. The operating principle of ALD is a gas phase–solid reaction between the evaporated metal-containing precursor and the substrate of a reduced pressure of 0.5 to 1 kPa. Precursor molecules attach on

the surface by chemisorption forming a homogeneous monolayer during one reaction cycle under ideal reaction conditions. The advantage of the ALD method is that highly dispersed homogeneous surfaces can be obtained due to the self-limiting nature of the ALD process.¹⁵

One of the main current applications of ALD is in the fabrication of semiconductor devices.¹⁶ However, this method has also been studied for coating different kinds of surfaces, both thin films on planar substrates and on porous materials;¹⁷ one example of these is catalysts.

In catalysis, ALD is a suitable preparation method because the resulting catalyst has good dispersion of the active particles on the support.¹⁸ This good dispersion enables a decreasing of the metal loading while still achieving the same activity as with catalysts with higher metal loading prepared by other methods. This is especially important with noble metal materials where the excess use of initial material should be avoided. ALD has been used successfully in the preparation of well-dispersed porous catalysts on oxide supports^{19,20} and on carbon nanomaterials.²¹ In fuel cell applications, the stability and the dispersion of the catalytically active phase are essential factors for optimizing the power densities of cells. ALD has been previously used to prepare fuel cell catalysts on various substrates like thin film carbon nanotube mats,²² carbon nanotubes,²³ and silicon.²⁴ However, ALD-prepared fuel cell catalysts on porous carbon powder support materials have not been studied.

Received: August 30, 2011

Published: October 24, 2011

In this work, the suitability of using ALD to prepare monometallic palladium catalysts on a porous carbon support for alcohol oxidation in alkaline media is investigated. Electrochemical activity for ethanol and isopropanol oxidation is determined in an electrochemical cell with a commercially available alkaline ionomer that can be also utilized in an alkaline DAFC. The results are compared with those obtained with a commercially available carbon-supported palladium catalyst.

■ EXPERIMENTAL METHODS

Chemicals and Materials. 1-Methyl-2-pyrrolidione (Sigma-Aldrich), NaOH (Merck), ethanol (Altia), iso-propanol (Merck), Pd(thd)₂ (2,2,6,6-tetramethyl-3,5-heptane dionate, Volatec Oy), FAA-2 solution (FumaTech), Vulcan XC72R (Cabot GR-3875), and Pd/C (Alfa Aesar) were used as received and were of analytical grade. Gases (N₂, synthetic air, CO) were all produced by AGA with at least 99.99% purification. Ion-exchanged Millipore Milli-Q water (0.04 $\mu\text{S cm}^{-1}$) was used while preparing solutions. Prior to experiments all glassware was purified in 0.05 M KMnO₄ (Merck) solution and rinsed with a solution containing diluted H₂O₂ (Sigma-Aldrich) and HClO₄ (Merck). After this procedure, the glassware was boiled and rinsed repeatedly with Milli-Q water.

Preparation of the Pd Catalysts. Catalyst preparation was carried out in a commercial flow-type F-120 ALD reactor (ASM Microchemistry) operating in a reduced pressure of 0.5 to 1 kPa. Catalyst preparation included three steps: (1) support pretreatment, (2) reaction of the evaporated precursor with the support, and (3) removal of precursor ligands from the surface. The catalyst support carbon (Vulcan XC72R) was pretreated in N₂ flow at 180 °C for 5 h. Precursor Pd(thd)₂ was fed through the catalyst support with nitrogen as carrier gas at 180 °C for 6 h per cycle. To ensure full surface saturation of the catalyst support bed, long precursor feed cycles and an excess amount of precursor were used. Reaction cycles were repeated until the desired metal content on the surface was achieved. The ALD reaction cycles were repeated four times. Thereafter, the unreacted precursor was flushed from the reactor with nitrogen, and ligands were removed from the surface by synthetic air. The reactor was cooled in nitrogen flow. A commercial reduced palladium catalyst on carbon black was used as a reference material (Pd loading 20 wt %).

Physical Characterization. The ALD-prepared catalyst was characterized by atomic emission spectroscopy (AES) (ICP-AES, Varian Liberty series II), X-ray diffraction, (XRD) (PanAnalytical X'Pert Pro), X-ray photoelectron spectroscopy (XPS) (SSX-100), transmission electron microscopy (TEM) (Tecnai 12 Bio Twin with LaB₆ gun at 120 kV), and scanning electron microscopy (SEM) equipped with energy-dispersive spectroscopy (EDS) (JEOL JSM-7500FA). AES and EDS were used for measuring the catalyst metal content. XRD and XPS were used for determining the oxidation states of metals on the catalysts. TEM and EDS were used for imaging the catalyst metal distribution. The metal particle size was calculated from TEM images. The commercial Pd/C catalyst was characterized by XRD and TEM, and the metal content was provided by the manufacturer.

Electrochemical Characterization. The electrode inks were prepared by mixing 5 mg of Pd/C catalyst, 200 μL of 1-methyl-2-pyrrolidione, and 20 μL of alkaline ionomer FAA-2 solution (5 wt %). After vigorous stirring on a magnetic stirrer, 5 μL of ink was dropped on a glassy carbon electrode surface cleaned by

alumina slurry and sonication in MQ water. The ink was dried in a vacuum oven at 70 °C to remove the solvent. This electrode was used as a working electrode in a three-electrode electrochemical cell, with temperature control. A large platinum coil was used as a counter electrode, and a mercury oxide electrode (MOE) was used as a reference. The potentials were scaled to correspond to the reversible hydrogen electrode (RHE). The measurements were performed with a PGSTAT100 Autolab system, and the working electrode was connected to an analytical rotator (Pine Instruments). Electrode characterization was performed in deaerated 0.1 M NaOH electrolyte that was heated to a stable value of 30 ± 0.5 °C. A clean electrode surface was obtained by CO adsorption/oxidation, where CO gas was purged into the cell for 2 h while the potential of the electrode was held at 0.1 V versus RHE. While maintaining the potential, the gas was switched to N₂ and purged for 40 min to remove CO from the electrolyte. Oxidation of the adsorbed CO was detected with cyclic voltammetry, and after this procedure electrode characterization was performed at the cleaned electrode surface. All currents in the Figures are scaled with the loading of the electrode.

The EASA was not determined from the hydrogen adsorption region because this region cannot be accurately determined on a palladium surface and some hydrogen can penetrate into the palladium lattice structure.^{25,26} Instead the EASA can be estimated from the palladium oxide reduction peak observed in cyclic voltammetry in alkaline solutions.^{25,27–29} Oxygen was assumed to form a monatomic layer prior to oxygen evolution,³⁰ therefore, the surface coverage of oxygen at the reduction peak (0.68 V vs RHE) was assumed to be 1. The value for EASA was determined with the following equation

$$S = \frac{Q_{\text{PdO}}}{\theta \cdot Q_{\text{PdO, mono}}} \quad (1)$$

where Q_{PdO} is the integrated area under the PdO peak, with the same integration limits used for all samples, θ is the surface coverage of oxygen, and $Q_{\text{PdO, mono}}$ is the charge value for the PdO reduction (a value of 405 $\mu\text{C cm}^{-2}$ was used³¹). The EASA values obtained were not used to scale the currents to current densities because of a lack of accuracy: the obtained value depends on the time of anodization, affecting the oxide thickness.^{32,33} Nevertheless, the experimental method was the same for all samples; therefore, these EASAs are internally comparable.

Alcohol Oxidation. After electrode cleaning and EASA characterization a solution containing 0.1 M NaOH and 1 M of ethanol or iso-propanol was placed into the cell. To minimize changes in alcohol concentration, the nitrogen inlet was first directed into a bubbler bottle containing the same solution as in the cell, and alcohol-saturated gas was directed to the experimental cell. The activity for alcohol oxidation was examined with both cyclic voltammetry and chronoamperometry to obtain information on the onset potential of alcohol oxidation and poisoning of the catalyst surfaces by reaction intermediates, respectively. The voltammograms were first recorded without rotation and after that with 1800 rpm rotation of the working electrode to ensure that mass transportation limitations did not occur. The currents presented in Figures are divided by the loading of the catalyst on the electrode. All voltammograms refer to the features in the third cycle, where reproducible response was attained.

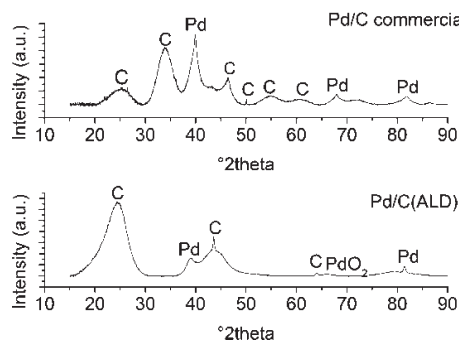


Figure 1. X-ray diffractograms of Pd/C(ALD) catalyst and Pd/C commercial catalysts.

RESULTS AND DISCUSSION

Physical Characterization. The metal loading of the ALD-prepared catalyst was determined by AES and EDS. According to the AES analysis, the palladium loading was 3.5 wt %, whereas in EDS analysis it was found to be 3.9 wt %. The metal loading from AES is presumably lower than that from EDS characterization because in AES the metal loading is determined from the whole sample, which is dissolved in acid, whereas in EDS the metal loading is determined from the upmost layer ($\sim 1 \mu\text{m}$). Therefore, values from AES and EDS characterization may differ from each other, if active metals are not evenly distributed throughout the whole thickness of catalyst. However, in our case, the values were close to each other and we can conclude that the active metal can be evenly distributed on porous substrate of the catalysts prepared with ALD method. The value determined by AES analysis was used to calculate the metal loading on the working electrode because catalytic oxidation takes place on the whole catalyst not only on the upmost layer of the catalyst. On commercial Pd/C catalyst used as a reference material metal loading was 20 wt %.

XPS and XRD were used for analyzing the metal oxidation states on the ALD-prepared catalyst. On the basis of XPS (Figure S1, Supporting Information) for the Pd/C(ALD) catalyst palladium is present both as palladium oxide (PdO_2) and metallic palladium.³⁴ Figure 1 presents X-ray diffractograms of the ALD-prepared and commercial catalysts. Peaks at 2θ positions 40.4, 68.4, and 82.4° indicate metallic palladium corresponding to $\text{Pd}(1\ 1\ 1)$, $(2\ 2\ 0)$, and $(2\ 2\ 2)$ planes, respectively. Metallic palladium is detected on both the commercial Pd/C and the Pd/C(ALD) catalyst. In Pd/C(ALD) X-ray diffractogram (Figure 1), there is also a small reflection detected at 2θ position around 67° corresponding to $\text{PdO}_2(1\ 1\ 2)$. This is in agreement with the XPS result, which indicated the presence of both metallic Pd and PdO_2 in the Pd/C(ALD) catalyst. XRD diffractograms of the catalyst support (Figure 1) were determined by measuring the pure support material prior to deposition of the metal. The catalyst support has exhibited peaks at angles of 24.6, 35.4, 43.6, 63.9, and 81.3°.

TEM images are presented in Figure 2, and they have been used for imaging the metal distribution and for particle sizes analysis of the samples. On the Pd/C(ALD) catalyst the mean particle size is 2.6 nm with standard deviation of 1.3 nm and on commercial Pd/C catalyst, 3.4 and 1.3 nm, respectively. From Figure 2, it can also be seen that the nanoparticles formed with the ALD method are evenly distributed throughout the supporting material and only a few aggregates are observed. However, with the commercial palladium catalyst, larger average particle

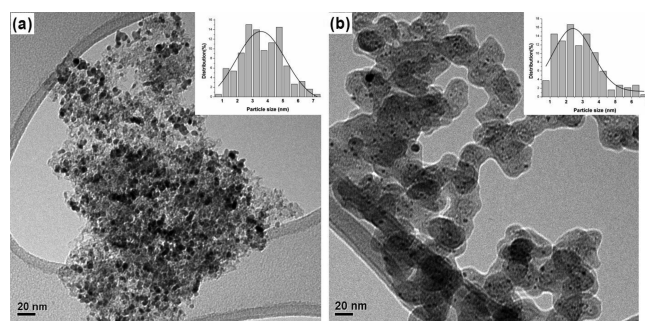


Figure 2. TEM images of Pd/C(Com) (a) and Pd/C(ALD) (b) with the histograms.

sizes can be observed, and this will strongly reduce the active surface area of the catalyst for the same metal loading.

To study the distribution of palladium on the carbon support in the ALD prepared catalyst, we have analyzed a rectangular area with sides of 23 and 31 μm using EDS. The SEM image of the surface of the sample and the corresponding analysis of carbon and palladium distribution are presented in Figure 3. From these images, it can be clearly seen that both the carbon used as the support material and palladium metal are very evenly distributed throughout the large sample. This confirms that with an ALD preparation method very uniform nanoparticle layers can be formed on the carbon support increasing strongly the catalytically active surface area of the metal.

Electrochemical Characterization. Prior to the electrochemical experiments the catalyst materials has been cleaned with the CO adsorption/oxidation method to ensure a clean catalyst surface without cycling to high voltages that might change the electrode surface construction. Cyclic voltammograms with cleaned electrode surfaces are presented in Figure 4. Even though hydrogen absorption into the palladium lattice occurs mainly for large particles and at a lower extent in nanoparticles,³⁵ the lower voltammogram limit has been selected to be 0.05 V, where no strong hydrogen absorption occurs. The cathodic peak at 0.2 V observed with both materials in Figure 4 is due to hydrogen adsorption on the surface atoms of the palladium nanoparticles,³⁶ and oxidation of this surface adsorbed hydrogen is observed in anodic peak between 0.2 and 0.3 V.^{35,37} The commercial catalyst material has less sharp peaks than the ALD prepared one, and its voltammogram corresponds more to bulk palladium behavior reported previously.³⁷ The second anodic peak between 0.3 and 0.5 V, partially overlapping the hydrogen region,³⁸ corresponds to OH^- adsorption from the alkaline electrolyte;³⁷ therefore, no thin double-layer region is observed, as is the case in acid media.^{35,39,40} When the working electrode is pushed to more anodic potentials (~ 0.6 V), the formation of a palladium oxide layer initiates and the corresponding oxide layer reduction can be seen between potentials of 0.8 to 0.4 V on the cathodic sweep.^{32,37,38,41} These palladium oxide formation and reduction peaks can be split into two subpeaks,³² which can be seen with Pd/C(ALD) catalyst in Figure 4; however, the mechanism is not understood in detail.

The magnitude of the catalyst material EASA can be estimated from the cyclic voltammograms (Figure 4) based on the charge needed for PdO reduction at the cathodic sweep. As already described in the Experimental Section, this is not as accurate as the method for determination of EASA with hydrogen adsorption on Pt surfaces; however, it is possible to obtain values for differently

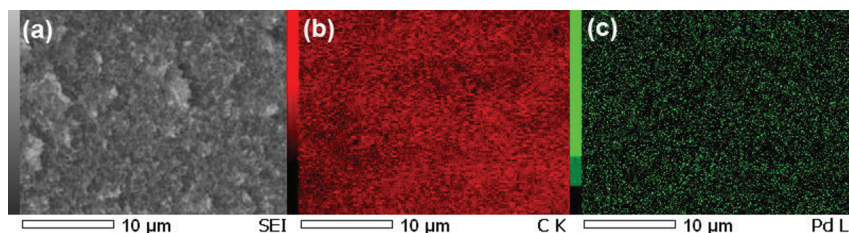


Figure 3. SEM image of the Pd/C(ALD) surface (a) and the element analysis by EDS: distribution of carbon (b) and palladium (c) on the surface.

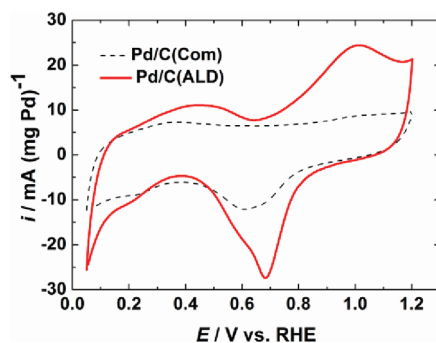


Figure 4. Cyclic voltammogram of the commercial and ALD prepared palladium materials in 0.1 M NaOH electrolyte with 20 mV s^{-1} sweep rate.

Table 1. Voltammetric Characteristics and EASA of Pd Catalysts Materials

material	$E_{\text{onset}}/\text{mV}^a$	E_p/mV^b	$I_{\text{pf}}/\text{mA}^c$	$I_{\text{pb}}/\text{mA}^c$	$\text{EASA}/\text{cm}^2^e$
Pd/C(Com)	EtOH	360	1200	348	45.8
Pd/C(Com)	PrOH	230	1200	493	39.3
Pd/C(ALD)	EtOH	300	890	894	1082
Pd/C(ALD)	PrOH	180	937	1247	1023

^a Onset potential. ^b Peak potential forward scan. ^c Mass activity forward scan. ^d Mass activity reverse scan. ^e Electrochemically active surface area.

prepared samples to compare the effect of preparation method. The calculated EASA values for all samples are presented in Table 1. As can be seen from Figure 4 and Table 1 the EASAs of the commercial Pd catalyst are significantly lower than the ones obtained with Pd/C(ALD) catalyst per mass of palladium. The commercial catalyst has similar EASA values to other commercial products.^{25–28} However, the values obtained with the Pd/C(ALD) catalyst are clearly higher. This would confirm that ALD deposition of palladium results in smaller particles, providing larger active catalyst area compared with the commercial catalyst, as has been seen already in physical characterization (Figures 2 and 3). This implies that ALD is a good method for preparing high active surface area catalysts on porous support and potentially reduces the amount of noble metal needed to provide high current densities.

To ensure that the catalyst has a clean surface after material synthesis, we have exposed the electrodes to CO gas. This is known to adsorb strongly on noble metal surfaces removing other compounds from the surface. When the electrode is cycled to higher potentials CO will oxidize to CO_2 , leaving the surface

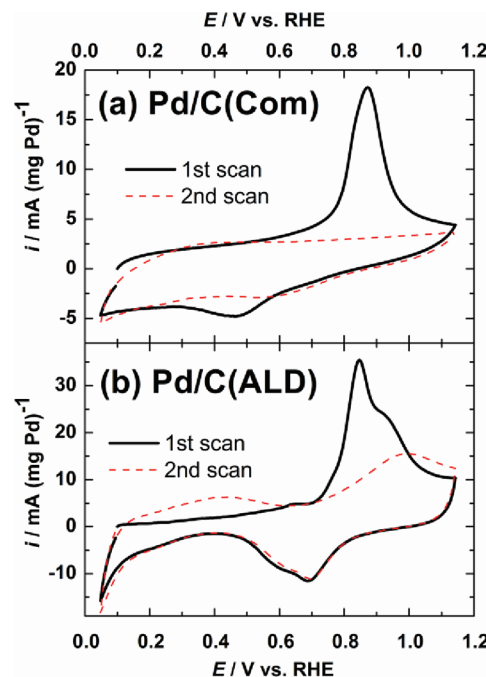


Figure 5. Cyclic voltammograms of preadsorbed (at 0.1 V potential) CO oxidation on the commercial palladium (a) and on the ALD-prepared Pd (b) in 0.1 M NaOH electrolyte, 10 mV s^{-1} . CO gas has been purged to the solution for 2 h and followed by purging with N₂ to eliminate CO from the electrolyte.

clean for studying the electrode properties. This CO stripping on both studied electrodes is presented in Figure 5, and the voltammograms show a sharp CO oxidation peak similar to other Pd-based catalysts in alkaline media.^{29,42} On the commercial catalyst CO oxidation occurs at a potential of 0.87 V (Figure 5); however, on the Pd/C(ALD) catalyst, there is one main peak at a slightly lower potential (0.84 V) and two shoulders at potentials of 0.64 and 0.92 V. The presence of shoulders commonly indicates that there are different surface sites where the CO has been adsorbed and the oxidation occurs at different potentials on these surface sites. Metallic nanoparticles have more surface sites and therefore more specific peaks than larger bulk-like particles. Sharper peaks obtained for ALD prepared catalyst in Figure 5 would imply that this catalyst is as small nanoparticles instead of larger particles, as has been confirmed by TEM and SEM images (Figures 2 and 3). Furthermore, strongly adsorbed CO will inhibit OH^- adsorption on the surface during the first scan; however, during the second scan a large OH^- adsorption on the totally cleaned surface can be clearly observed especially with the ALD prepared catalyst (Figure 5).

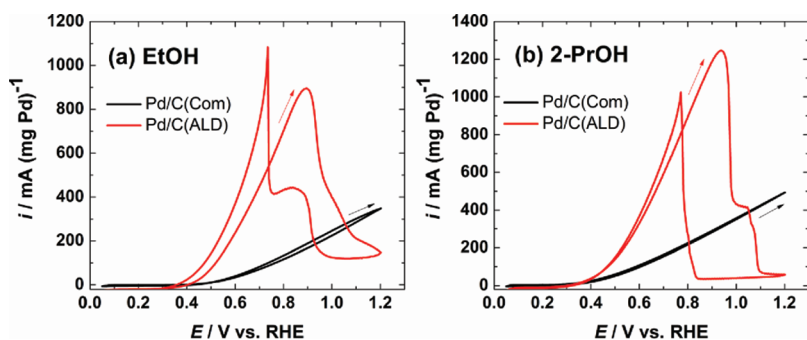


Figure 6. Ethanol (a) and isopropanol (b) oxidation in solution containing 0.1 M NaOH and 1 M of the studied alcohol with 1800 rpm rotation and 10 mV s^{-1} . The third scan is presented and the arrows indicate the forward scan of the voltammograms.

Alcohol Oxidation. Ethanol and isopropanol oxidation on the ALD-prepared Pd catalyst material has been studied with a rotating disk electrode and compared with the values obtained with the commercial catalyst material (Figure 6). In Table 1 for the onset potential of alcohol oxidation as well as the main peak potentials and peak currents are presented. These currents are divided by the palladium loading on the electrode and therefore referred to the mass activity of the catalyst. The onset of ethanol oxidation occurs at 360 mV on the Pd/C(Com) surface and is shifted to 60 mV more negative potentials on the Pd/C(ALD) catalyst. This indicates that smaller particle size of this catalyst is favorable for the first oxidation step of ethanol. The onset potential is in agreement with the results obtained by other groups.^{3,10,27,37,42–44} For ethanol oxidation a clear oxidation peak is obtained on Pd/C(ALD) catalyst at 890 mV (Figure 6a and Table 1); however, for the commercial catalyst the reaction proceeds moderately and therefore no oxidation peak is observed. Nevertheless, when the working electrode has not been rotated the limiting current will be reached earlier, and oxidation peaks for both alcohols are observed on all surfaces (Supporting Information, Figure S2). It can be clearly seen from Figure 6 that ethanol oxidation is very efficient on Pd/C(ALD) catalyst, and high currents are obtained already at low potentials, which is vital for lowering the fuel cell anode potential. At 890 mV the catalyst surface is covered with an intermediate product of ethanol oxidation, most likely acetate,^{10,45} which inhibits further ethanol adsorption on the surface. At slightly higher potentials there is a plateau where the oxidation would seem to proceed somewhat further; this might indicate minor carbonate formation, as previously observed with FTIR experiments.⁴⁵ On the return scan two separate peaks at 844 and 735 mV are observed (Figure 6) that are normally related to the removal of carbonaceous species, which have not been totally oxidized in the forward scan.^{46,47} The maximum mass activity obtained with commercial material is 348 mA ($\text{mg Pd})^{-1}$, which correlates well with the values obtained by other groups for similar materials on a Vulcan support.^{48,49} However, the mass activity on the Pd/C(ALD) catalyst is more than 2.5 times higher compared with the commercial catalyst. This indicates that the nanoparticles prepared by the ALD method provide a wide selection of suitable catalyst sites for ethanol oxidation.

Similar phenomena are observed with isopropanol oxidation on both Pd catalysts (Figure 6b): the onset potential for oxidation shifts to 50 mV lower potential with the Pd/C(ALD) catalyst compared with the commercial one. On the Pd/C(ALD) catalyst, oxidation is very efficient until 937 mV where the surface

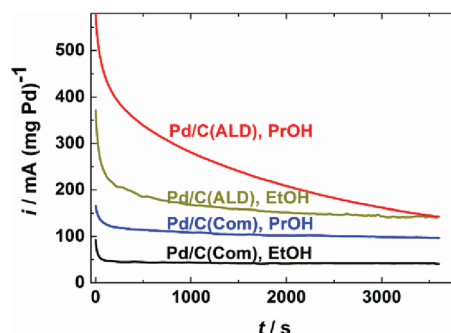


Figure 7. Chronoamperometric curves for 1 M alcohol in 0.1 M NaOH electrolyte at 0.7 V versus RHE potential.

is totally blocked by the isopropanol intermediate acetone;¹⁰ however, at higher potential (1040 mV) a small shoulder is observed, indicating that further oxidation does occur on this catalyst. This phenomenon is not observed on the commercial catalyst even when the working electrode is not rotating and the current maximum is reached (Supporting Information, Figure S2). This would indicate that the ALD-prepared catalyst would offer a different type of surface sites also for isopropanol oxidation. With the return scan the surface regains full activity at ~ 800 mV potential when PdO starts to reduce (Figure 4) and isopropanol adsorption on the surface can continue. This behavior of the voltammogram has been reported by other groups on bulk Pd electrode and electrodeposited Pd.^{50,51} The mass activity of isopropanol oxidation is very high on the Pd/C(ALD) material (1247 mA ($\text{mg Pd})^{-1}$) that is also ~ 2.5 times higher than on commercial catalyst and ~ 40 times higher than reported by Zhou et al.⁵⁰ for electrodeposited palladium on a glassy carbon electrode. This underlines the high activity of nanoparticle catalyst materials, especially ones prepared using the ALD method.

In a working fuel cell system the current is withdrawn at constant potential rather than cycling; therefore, also chronoamperometric curves have been recorded at 0.7 V potential (Figure 7), where all of the catalyst considered shows significant alcohol oxidation. On all catalyst surfaces the initial mass activity observed in cyclic voltammograms (Figure 6) decreases rapidly due to surface poisoning with the reaction intermediates: acetate for ethanol and acetone for isopropanol oxidation.¹⁰ Nevertheless, with the Pd/C(ALD) catalyst higher currents are maintained with both alcohols compared with the commercial Pd catalyst. This would imply that the Pd/C(ALD) catalyst is more tolerant to surface poisoning at least for 1 h experiments.

When the oxidation of these two alcohols is compared (Figure 6 and 7) it can be clearly seen that the isopropanol oxidation initiates 120 mV earlier compared with ethanol oxidation, as has been previously reported by Su et al.⁵² This indicates that isopropanol is an interesting fuel for an alkaline DAFC because it can be oxidized on Pd at lower potentials. In addition, isopropanol oxidation provides >350 mA (mg Pd) $^{-1}$ higher maximum mass activity compared with ethanol oxidation (Figure 6 and Table 1). These results show that isopropanol oxidation would benefit from well-distributed Pd nanoparticle catalyst material even more than ethanol. Therefore, from the chronoamperometric experiments in Figure 7 it can be clearly seen that surface poisoning is a vital issue in isopropanol oxidation, and one option to overcome this may be to alloy Pd with another metal that could further oxidize the acetone produced. In the future, this alloying could result in the higher performance of both ethanol and isopropanol oxidation needed for the commercialization of the alkaline DAFCs.

CONCLUSIONS

In this Article, we demonstrate that a Pd nanoparticle catalyst on a porous carbon support can be prepared with ALD. The particle size distribution of this material is narrow, and the particles formed are evenly distributed on the support material providing a high surface area for alcohol oxidation. This catalyst showed superior performance in both ethanol and isopropanol oxidation in alkaline media compared with a similar commercial material. In particular, the onset potential of oxidation for both alcohols shifted from 50 to 60 mV more negative potentials providing high mass activity already at low potentials, which is vital for DAFC operation. In addition, maximum mass activities obtained with the Pd/C(ALD) catalysts are ~ 2.5 times higher compared with the commercial material, enabling a decrease in the catalyst loading that could significantly lower the cost of the fuel cell electrode materials. Nevertheless, catalyst poisoning by oxidation reaction intermediates still remains a serious obstacle and will be addressed in future work.

ASSOCIATED CONTENT

S Supporting Information. Additional figures of the XPS spectrum as well as alcohol oxidation with and without rotation of the working electrode. This material is available free of charge via the Internet at <http://pubs.acs.org>.

AUTHOR INFORMATION

Corresponding Author

*Tel: +358 9 470 22 618. Fax: +358 9 470 22622. E-mail: emma.rikkinen@aalto.fi.

ACKNOWLEDGMENT

CNB-E project through the Multidisciplinary Institute of Digitalization and Energy (MIDE) program and Academy of Finland are acknowledged for financial support.

REFERENCES

- (1) Lamy, C.; Belgsri, E. M.; Leger, J.-M. *J. Appl. Electrochem.* **2001**, *31*, 799–809.
- (2) Jiang, L.; Hsu, A.; Chu, D.; Chen, R. *Int. J. Hydrocarbon Eng.* **2010**, *35*, 365–372.
- (3) Dimos, M. M.; Blanchard, G. J. *J. Phys. Chem. C* **2010**, *114*, 6019–6026.
- (4) Lai, S. C. S.; Koper, M. T. M. *Phys. Chem. Chem. Phys.* **2009**, *11*, 10446–10456.
- (5) Fujiwara, N.; Siroma, Z.; Yamazaki, S.; Ioroi, T.; Senoh, H.; Yasuda, K. *J. Power Sources* **2008**, *185*, 621–626.
- (6) Danks, T. N.; Slade, R. C. T.; Varcoe, J. R. *J. Mater. Chem.* **2002**, *12*, 3371–3373.
- (7) Varcoe, J. R.; Slade, R. C. T.; Yee, E. L. H.; Poynton, S. D.; Driscoll, D. J.; Apperley, D. G. *Chem. Mater.* **2007**, *19*, 2686–2693.
- (8) Wang, G.; Weng, Y.; Chu, D.; Chen, R.; Xie, D. *J. Membr. Sci.* **2009**, *332*, 63–68.
- (9) Santasalo-Aarnio, A.; Hietala, S.; Rauhala, T.; Kallio, T. *J. Power Sources* **2011**, *196*, 6153–6159.
- (10) Santasalo-Aarnio, A.; Kwon, Y.; Ahlberg, E.; Kontturi, K.; Kallio, T.; Koper, M. T. M. *Electrochem. Commun.* **2011**, *13*, 466–469.
- (11) Xu, C. W.; Cheng, L. Q.; Shen, P. K.; Liu, Y. L. *Electrochem. Commun.* **2007**, *9*, 997–1001.
- (12) Santasalo-Aarnio, A.; Peljo, P.; Aspberg, E.; Kontturi, K.; Kallio, T. *ECS Trans.* **2010**, *33*, 1701–1714.
- (13) Qi, Z.; Kaufman, A. *J. Power Sources* **2002**, *112*, 121–129.
- (14) Bambagioni, V.; Bianchini, C.; Marchionni, A.; Filippi, J.; Vizza, F.; Teddy, J.; Serp, P.; Zhiani, M. *J. Power Sources* **2009**, *190*, 241–251.
- (15) Puurunen, R. L. *J. Appl. Phys.* **2005**, *97*, 121301–1 – 121301–52.
- (16) George, S. M. *Chem. Rev.* **2010**, *110*, 111–131.
- (17) Ritala, M.; Leskelä, M. *Handbook of Thin Film Materials*; Nalwa, H. S., Ed.; Academic Press: San Diego, 2002; Vol. 1
- (18) Puurunen, R. L. *J. Appl. Phys.* **2005**, *97*, 121301–1 – 121301–52.
- (19) Silvennoinen, R.; Jylhä, O. J. T.; Lindblad, M.; Sainio, J. P.; Puurunen, R. L.; Krause, A. O. I. *Appl. Surf. Sci.* **2007**, *253*, 4103–4111.
- (20) Vuori, H.; Silvennoinen, R. J.; Lindblad, M.; Österholm, H.; Krause, A. O. I. *Catal. Lett.* **2009**, *131*, 7–15.
- (21) Plomp, A. J.; Vuori, H.; Krause, A. O. I.; de Jong, K. P.; Bitter, J. H. *Appl. Catal., A* **2008**, *351*, 9–15.
- (22) Bult, J.; Dameron, A.; Pylypenko, S.; Engrakul, C.; Bochert, C.; Chen, L.; Leong, G.; Frisco, S.; Simpson, L.; Dinh, H. N.; Pivoar, B. *ECS Trans.* **2010**, *33*, 89–96.
- (23) Liu, C.; Wang, C.-C.; Kei, C.-C.; Hsueh, Y.-C.; Perng, T.-P. *Small* **2009**, *5*, 1535–1538.
- (24) Jiang, X.; Gür, T. M.; Prinz, F. B.; Bent, S. F. *Chem. Mater.* **2010**, *22*, 3024–3032.
- (25) Pattabiraman, R. *Appl. Catal., A* **1997**, *153*, 9–20.
- (26) Lukaszewski, M.; Grden, M.; Czerwinski, A. *J. Solid State Electrochem.* **2005**, *9*, 1–9.
- (27) Ottakam Thotiyil, M. M.; Ravi Kumar, T.; Sampath, S. *J. Phys. Chem. C* **2010**, *114*, 17934–17941.
- (28) Zhao, Y.; Yang, X.; Tian, J.; Wang, F.; Zhan, L. *Int. J. Hydrogen Energy* **2010**, *35*, 3249–3257.
- (29) Modibedi, R. M.; Masombuka, T.; Mathe, M. K. *Int. J. Hydrogen Energy* **2011**, *36*, 4664–4672.
- (30) Michri, A. A.; Pshchenicknikov, A. G.; Burshtein, R. Kh. *Elektrokhimiya* **1972**, *8*, 364–366.
- (31) Chierchie, T.; Mayer, C.; Lorenz, W. J. *J. Electroanal. Chem.* **1982**, *135*, 211–220.
- (32) Takamura, T.; Mochimaru, F. *Electrochim. Acta* **1969**, *14*, 111–119.
- (33) Trasatti, S.; Petrii, O. A. *J. Electroanal. Chem.* **1992**, *327*, 353–376.
- (34) Moulder, J. F. *Handbook of X-ray Photoelectron Spectroscopy: A Reference Book of Standard Spectra for Identification and Interpretation of XPS Data*; Perkin-Elmer: Eden Prairie, MN, 1992.
- (35) Pan, W.; Zhang, X.; Ma, H.; Zhang, J. *J. Phys. Chem. C* **2008**, *112*, 2456–2461.
- (36) Grden, M.; Piascik, A.; Koczorowski, Z.; Czerwinski, A. *J. Electroanal. Chem.* **2002**, *532*, 35–42.
- (37) Liang, Z. X.; Zhao, T. S.; Xu, J. B.; Zhu, L. D. *Electrochim. Acta* **2009**, *54*, 2203–2208.

- (38) Grden, M.; Czerwinski, A. *J. Solid State Electrochem.* **2008**, *12*, 375–385.
- (39) Birry, L.; Lasia, A. *Electrochim. Acta* **2006**, *51*, 3356–3364.
- (40) Guerin, S.; Attard, G. S. *Electrochem. Commun.* **2001**, *3*, 544–548.
- (41) Burke, L. D.; Casey, J. K. *J. Electrochem. Soc.* **1993**, *140*, 1292–1298.
- (42) Wang, Y.; Nguyen, T. S.; Liu, X.; Wang, X. *J. Power Sources* **2010**, *195*, 2619–2622.
- (43) Xu, C.; Liu, Y.; Yuan, D. *Int. J. Electrochem. Sci.* **2007**, *2*, 674–680.
- (44) Xu, J. B.; Zhao, T. S.; Shen, S. Y.; Li, Y. S. *Int. J. Hydrocarbon Eng.* **2010**, *35*, 6490–6500.
- (45) Zhou, Z.-Y.; Wang, Q.; Lin, J.-L.; Tian, N.; Sun, S.-G. *Electrochim. Acta* **2010**, *55*, 7995–7999.
- (46) Morin, M. C.; Lamy, C.; Léger, J. M. *J. Electroanal. Chem.* **1990**, *283*, 287–302.
- (47) Manoharan, R.; Goodenough, J. B. *J. Mater. Chem.* **1992**, *2*, 875–887.
- (48) Zhao, Y.; Zhan, L.; Tian, J.; Nie, S.; Ning, Z. *Int. J. Hydrocarbon Eng.* **2010**, *35*, 10522–10526.
- (49) Liu, Z.; Zhang, X.; Hong, L. *Electrochem. Commun.* **2009**, *11*, 925–928.
- (50) Zhou, W.; Wang, C.; Xu, J.; Du, Y.; Yang, P. *Mater. Chem. Phys.* **2010**, *123*, 390–395.
- (51) Liu, J.; Ye, J.; Xu, C.; Jiang, S. P.; Tong, Y. *J. Power Sources* **2008**, *177*, 67–70.
- (52) Su, Y.; Xu, C.; Liu, J.; Liu, Z. *J. Power Sources* **2009**, *194*, 295–297.